# Cystic Focal Liver Lesions in the Adult: Differential CT and MR Imaging Features[1]

*Koenraad J. Mortelé, MD • Pablo R. Ros, MD*

**ONLINE-ONLY CME**

*See www.rsna.org/education/rg_cme.html.*

**LEARNING OBJECTIVES**

*After reading this article and taking the test, the reader will be able to:*

- Describe a variety of cystic focal liver lesions in the adult.
- Recognize the features of these masses at evaluation with CT and MR imaging.
- List the differentiating clinical, radiologic, and histopathologic findings in cystic liver lesions in the adult.

Cystic lesions of the liver in the adult can be classified as developmental, neoplastic, inflammatory, or miscellaneous. Although in some cases it is difficult to distinguish these entities with imaging criteria alone, certain cystic focal liver lesions have classic computed tomographic (CT) and magnetic resonance (MR) imaging features, which are important for the radiologist to understand and recognize. Lesions with such features include simple (bile duct) cyst, autosomal dominant polycystic liver disease, biliary hamartoma, Caroli disease, undifferentiated (embryonal) sarcoma, biliary cystadenoma and cystadenocarcinoma, cystic subtypes of primary liver neoplasms, cystic metastases, pyogenic and amebic abscesses, intrahepatic hydatid cyst, extrapancreatic pseudocyst, and intrahepatic hematoma and biloma. Specific CT and MR imaging findings that are important to recognize are the size of the lesion; the presence and thickness of a wall; the presence of septa, calcifications, or internal nodules; the enhancement pattern; the MR cholangiographic appearance; and the signal intensity spectrum. In addition, access to critical clinical information remains extremely important. The most important clinical parameters defined include age and gender, clinical history, and symptoms. An understanding of the classic CT and MR imaging appearances of cystic focal liver lesions will allow more definitive diagnosis and shorten the diagnostic workup.

**Index terms:** Bile ducts, diseases, 761.288 • Liver, abscess, 761.21 • Liver, cysts, 761.312 • Liver, echinococcosis, 761.2083 • Liver, hemorrhage, 761.412 • Liver neoplasms, diagnosis, 761.314, 761.3194, 761.32 • Liver neoplasms, secondary, 761.33 • Pancreas, cysts, 770.291

**RadioGraphics 2001;** 21:895–910

[1]From the Department of Radiology, Brigham and Women's Hospital, Harvard Medical School, 75 Francis St, Boston MA 02115. Received December 29, 2000; revision requested March 1, 2001, and received March 21; accepted March 21. **Address correspondence to** K.J.M. (e-mail: *kmortele@partners.org*).

**Clinical, CT, and MR Imaging Features of Cystic Focal Liver Lesions**

| Type of Lesion | Critical Clinical Features | Key CT and MR Imaging Features |
|---|---|---|
| Developmental | | |
| Hepatic cyst | Asymptomatic, coexistence of renal cystic disease in ADPLD* | Homogeneous, round, regular, no wall, no enhancement |
| Bile duct hamartoma | Asymptomatic | Homogeneous, rim enhancement, all lesions smaller than 1.5 cm in diameter |
| Caroli disease | Asymptomatic or symptoms of cholangitis | Cysts communicating with the biliary tree, central dot sign, septa |
| Neoplastic | | |
| Undifferentiated sarcoma | Occurs in older children and young adults, symptomatic | Large solitary lesion, enhancing solid components, calcifications |
| Biliary cystadenoma or cystadenocarcinoma | Occurs in middle-aged women, usually symptomatic | Multilocular, mural nodules, fibrous capsule, calcifications, variable signal intensities |
| Hepatocellular carcinoma | Liver cirrhosis, history of embolization | Hypervascular solid part, capsule, signs of cirrhosis |
| Cavernous hemangioma | Asymptomatic | Peripheral nodular enhancement, large lesion |
| Cystic metastases | Known primary tumor (colorectal, sarcoma, carcinoid, etc) | Rim enhancement, multiple |
| Metastases from ovarian cancer | Known ovarian carcinoma | Capsular implants |
| Inflammatory | | |
| Abscess | Fever, sepsis | Presence of air, double target sign, enhancing wall |
| Hydatid cyst | Positive serologic results or clinical history | Calcifications, daughter cysts, pericyst |
| Miscellaneous | | |
| Subcapsular pseudocyst | Pancreatitis | Occurs in left liver lobe, signs of pancreatitis, thin capsule |
| Intrahepatic hematoma | Liver trauma, known hepatocellular adenoma | Fluid attenuation at CT, methemoglobin at MR imaging, signs of trauma |
| Intrahepatic biloma | Liver trauma, biliary surgery | No capsule, no septa, no calcifications |

*Autosomal dominant polycystic liver disease.

## Introduction

Cystic lesions of the liver in the adult can be classified as developmental, neoplastic, inflammatory, or miscellaneous lesions. Because the clinical implications of and therapeutic strategies for cystic focal liver lesions vary tremendously according to their causes, the ability to differentiate noninvasively all types of cystic tumors is extremely important. With the rapid advances in imaging techniques over the past 2 decades, including the development of both dynamic spiral computed tomography (CT) and fast magnetic resonance (MR) imaging and the ability to use tailored MR imaging techniques such as MR cholangiopancreatography, it is now possible to assess the morphologic and hemodynamic features of a vast array of liver tumors.

Several authors have tried to characterize cystic focal liver lesions on the basis of both quantitative data and qualitative observations (1–3). However, many overlapping characteristics were shown to exist among the various neoplasms; these overlapping characteristics frequently led to a long list of differential diagnoses with a subsequent lengthy and expensive work-up for the patient.

However, in the majority of cases, familiarity with the most relevant radiologic key features, in combination with critical clinical information, provides enough information for adequate lesion characterization. This article presents the characteristic CT and MR imaging findings of the gamut of both usual and unusual cystic focal liver lesions, along with their most relevant clinical differential points and in correlation with their histopathologic background (Table).

## Developmental Lesions

### Hepatic (Bile Duct) Cyst

Simple hepatic cysts are benign developmental lesions that do not communicate with the biliary tree (4). The current theory regarding the origin of true hepatic cysts is that they originate from

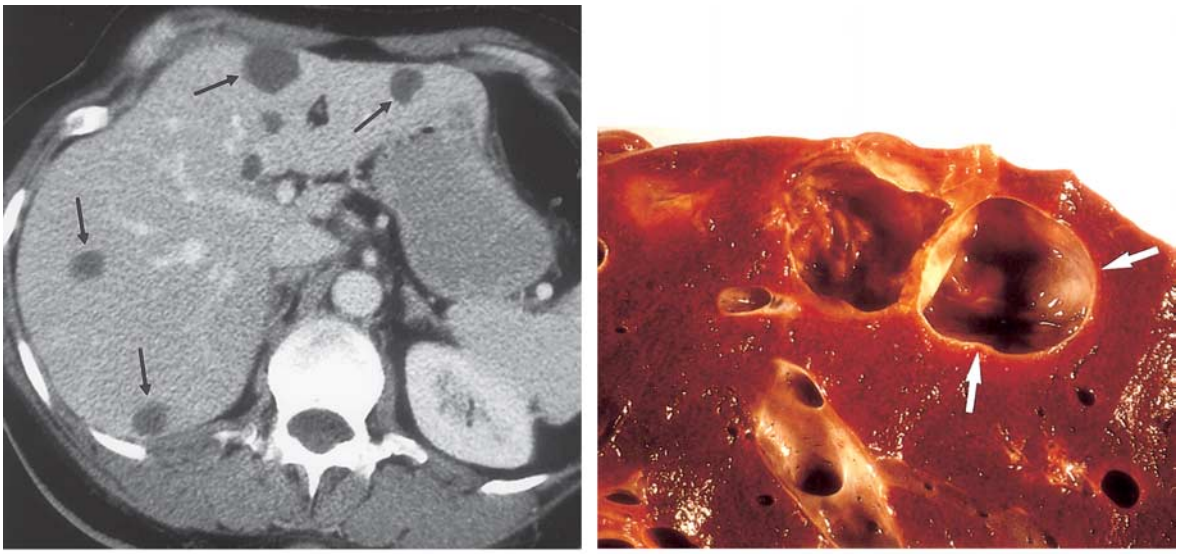

a. b.

**Figure 1.** Hepatic cysts in an asymptomatic 37-year-old woman. **(a)** Portal-venous-phase contrast material–enhanced CT scan shows multiple homogeneous, rounded, well-defined, nonenhancing cystic lesions (arrows), which are consistent with simple bile duct cysts. **(b)** Photograph of a hepatectomy specimen shows a thin-walled cystic lesion (arrows), which is compatible with a simple bile duct cyst.

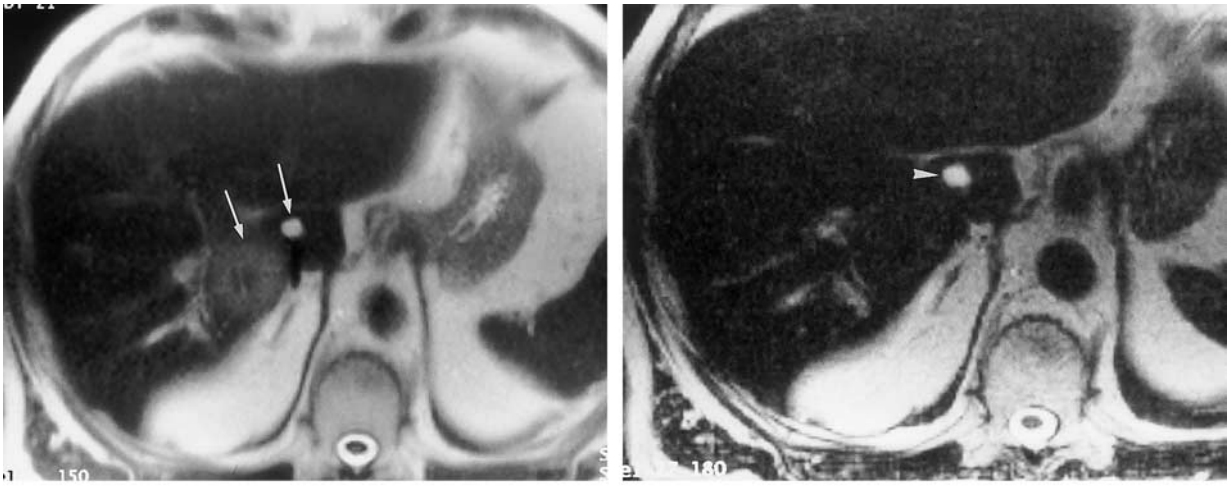

a. b.

**Figure 2.** Hepatic cyst in a patient with a history of colon carcinoma. **(a)** Fast spin-echo T2-weighted MR image shows two high-signal-intensity lesions (arrows) in segment 1 of the liver. **(b)** Heavily T2-weighted MR image (effective echo time, 166 msec) shows that only the smaller lesion (arrowhead) continues to have the signal intensity of fluid. Therefore, the larger lesion represents a metastasis and the smaller lesion represents a simple bile duct cyst.

hamartomatous tissue (4). Hepatic cysts are common and are presumed to be present in 2.5% of the population (5). They are more often discovered in women and are almost always asymptomatic (4,5). Simple hepatic cysts can be solitary or multiple, with the latter being the more typical scenario. At histopathologic analysis, true hepatic cysts contain serous fluid and are lined by a nearly imperceptible wall consisting of cuboidal epithelium, identical to that of bile ducts, and a thin underlying rim of fibrous stroma.

A hepatic cyst appears as a homogeneous and hypoattenuating lesion on nonenhanced CT scans, with no enhancement of its wall or content after intravenous administration of contrast material (Fig 1) (5). It is typically round or ovoid and well-defined (5). At MR imaging, hepatic cysts have homogeneous very low signal intensity on T1-weighted images and homogeneous very high signal intensity on T2-weighted images. Owing to their fluid content, an increase in signal intensity is seen on heavily T2-weighted images. This increase allows differentiation of these lesions from metastatic disease (Fig 2). No enhancement is seen after administration of gadolinium chelates.

In cases of intracystic hemorrhage, a rare complication in simple hepatic cysts, the signal intensity is high, with a fluid-fluid level, on both T1- and T2-weighted images when mixed blood products are present (5).

On the basis of these features, either CT alone or MR imaging alone is sufficient to establish an accurate diagnosis of a simple hepatic cyst in most cases.

## Polycystic Liver Disease

Hepatic cysts can also be part of polycystic liver disease, an autosomal dominant disorder often found in association with renal polycystic disease (4). Although hepatic cysts are found in 40% of cases of autosomal dominant polycystic disease involving the kidneys, they may be seen without identifiable renal involvement at radiography (1). Usually, patients with autosomal dominant polycystic liver disease are asymptomatic and liver dysfunction occurs only sporadically (4). However, advanced disease can result in hepatomegaly, liver failure, or Budd-Chiari syndrome. In these more severe cases, percutaneous interventional alcohol ablation has been useful as an alternative to partial liver resection or even transplantation (4).

Polycystic liver disease typically appears as multiple homogeneous and hypoattenuating cystic lesions with a regular outline on nonenhanced CT scans, with no wall or content enhancement on contrast-enhanced images (Fig 3). At MR imaging, hepatic cysts in polycystic liver disease have very low signal intensity on T1-weighted images and do not enhance after administration of gadolinium contrast material (Fig 4a). Owing to their pure fluid content, homogeneous high signal intensity is demonstrated on T2-weighted and heavily T2-weighted images (Fig 4b). In patients with polycystic liver disease, signal intensity abnormalities indicating intracystic hemorrhage are more frequently encountered than in cases of simple hepatic cysts due to the great number of cysts (5). Although the diagnosis of polycystic liver disease is easily made with both CT and MR imaging, MR imaging is more sensitive for the detection of complicated cysts.

## Bile Duct Hamartoma

Bile duct hamartomas, also called von Meyenburg complexes, originate from embryonic bile ducts that fail to involute (6–11). They are generally without clinical manifestations and are usually encountered as an incidental finding at imaging, laparotomy, or autopsy (6–11). At pathologic analysis, they appear as grayish-white nodular lesions 0.1–1.5 cm in diameter that do not communicate with the biliary tree and are scattered throughout the liver parenchyma (Fig 5a) (6).


a.

b.

**Figure 3.** Autosomal dominant polycystic kidney and liver disease in a 45-year-old patient. **(a)** Portal-venous-phase contrast-enhanced CT scan shows multiple nonenhancing hepatic and renal cysts (arrowheads). **(b)** Photograph of a hepatectomy specimen shows numerous thin-walled cystic lesions (arrows), which are compatible with polycystic liver disease.

In almost all reported cases, nonenhanced CT has shown multiple hypoattenuating, cystlike hepatic nodules occurring throughout both lobes of the liver and typically measuring less than 1.5 cm in diameter (7,8). The latter feature is the most essential one in the differential diagnosis from multiple simple cysts. Furthermore, simple cysts are typically regularly outlined, whereas bile duct hamartomas have a more irregular outline. Bile

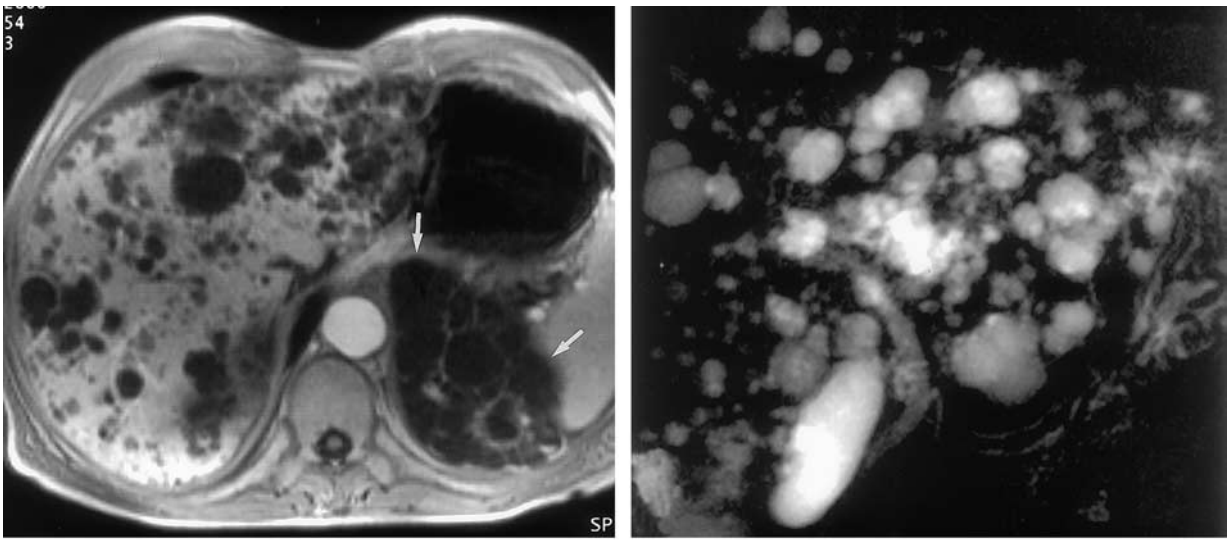


a. b.

**Figure 4.** Polycystic liver disease. **(a)** Arterial-phase gadolinium-enhanced T1-weighted MR image, obtained in a 23-year-old woman with autosomal dominant polycystic kidney and liver disease, shows renal cysts (arrows) and the typical MR imaging appearance of hepatic cysts: homogeneity, well-defined borders, and no enhancement of wall or content. **(b)** Coronal projection MR cholangiogram obtained in a 67-year-old patient shows numerous hyperintense cysts of varying size scattered throughout the liver. Note that the cystic lesions do not communicate with the biliary tree.

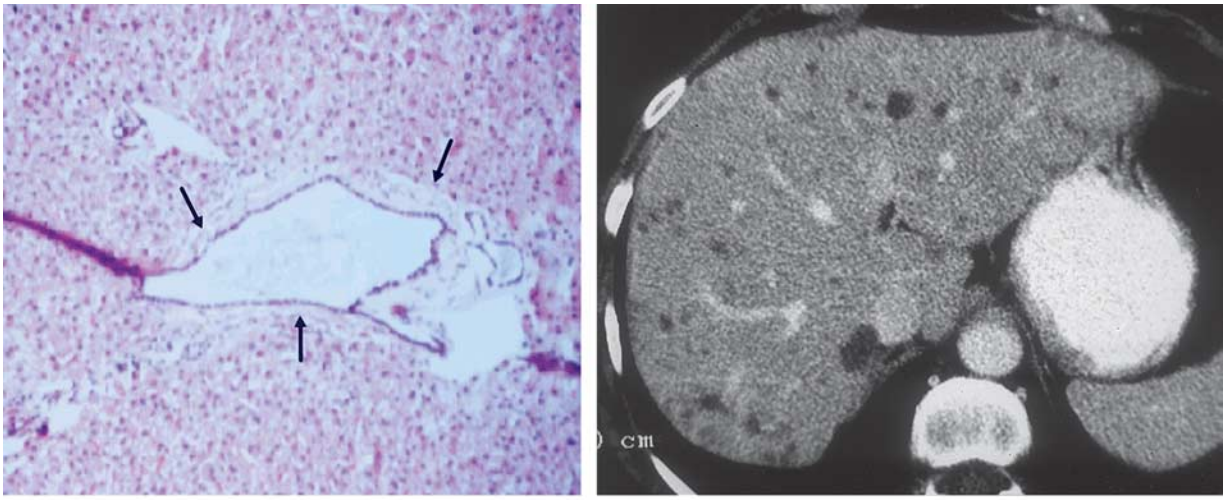

a. b.

**Figure 5.** Biliary hamartoma. **(a)** Photomicrograph of a liver biopsy specimen shows a centrally located cystic lesion with internal debris lined by a single layer of biliary epithelium (arrows). **(b)** Portal-venous-phase contrast-enhanced CT scan obtained in an asymptomatic 44-year-old woman shows numerous small cystic lesions scattered throughout the liver. No enhancement is seen.

duct hamartomas do not exhibit a characteristic pattern of enhancement after intravenous administration of iodinated contrast material. Although homogeneous enhancement of the lesions has been noted in some cases, in most reports no enhancement was seen on contrast-enhanced CT images (Fig 5b) (8,9,11).

The MR imaging appearance of bile duct hamartomas has been reported sporadically (9–11). All lesions were hypointense relative to liver parenchyma on T1-weighted images and strongly hyperintense on T2-weighted images (Fig 6a) (1,11). On heavily T2-weighted images, the signal intensity increases further, almost reaching the signal intensity of fluid (8,11). At MR cholangiography, bile duct hamartomas appear as multiple tiny cystic lesions that do not communicate with the biliary tree (Fig 6b). After intravenous

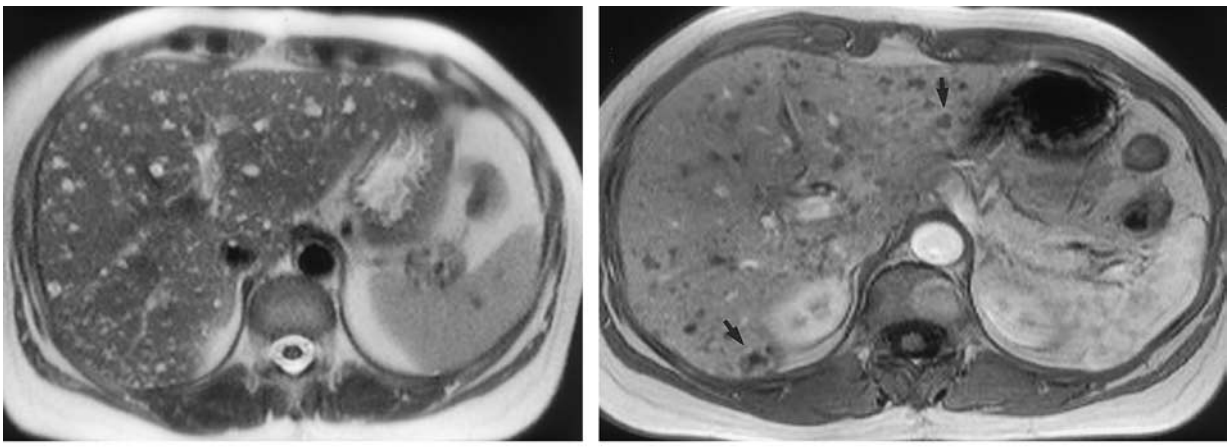

a. c.

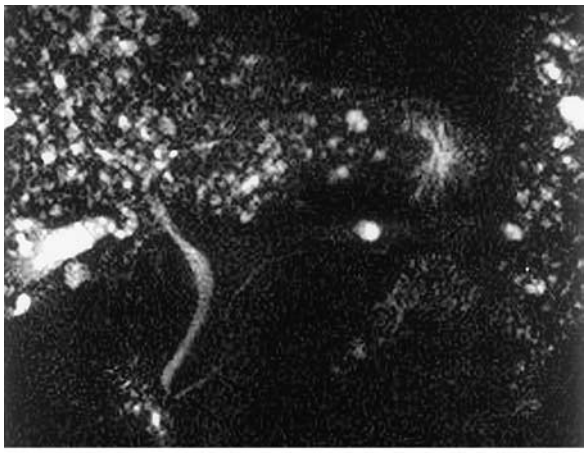

b.

**Figure 6.** Biliary hamartomas in a 32-year-old woman. **(a)** Fast spin-echo T2-weighted MR image shows multiple small (<1.5-cm-diameter), hyperintense nodules consistent with biliary hamartomas. **(b)** Coronal projection MR cholangiogram shows that all of the lesions are smaller than 1.5 cm in diameter and do not communicate with the biliary tree. **(c)** Arterial-phase gadolinium-enhanced T1-weighted MR image shows that some of the lesions have rimlike peripheral enhancement (arrows).

administration of gadolinium contrast material, some authors observed homogeneous enhancement of these lesions (1,8), whereas others did not find any enhancement (9). Recently, thin rim enhancement on gadolinium-enhanced images was reported in four cases (11) (Fig 6c). This rim enhancement was considered to correlate with the compressed liver parenchyma that surrounds the lesions at histopathologic analysis (11).

At both CT and MR imaging, multiple small (<1.5-cm-diameter) cystic lesions in the liver without renal involvement should favor the diagnosis of biliary hamartomas. However, MR imaging is superior to CT in demonstrating the cystic nature of the lesions.

## Caroli Disease

Caroli disease, also known as congenital communicating cavernous ectasia of the biliary tract, is a rare, autosomal recessive developmental abnormality characterized by saccular dilatation of the intrahepatic bile ducts, multiple intrahepatic calculi, and associated cystic renal disease (12–14). Two forms of Caroli disease have been described: a less common pure form (type 1) and a more complex form (type 2), which is associated with other ductal plate abnormalities, such as hepatic fibrosis (13). The abnormality may be segmental or diffuse. Clinical symptoms are usually restricted to recurrent attacks of right upper quadrant pain, fever, and, more rarely, jaundice (1). The prevalence of cholangiocarcinoma is higher in patients with this disease than in the general population (14).

CT typically shows hypoattenuating dilated cystic structures of varying size that communicate with the biliary tree (14). The presence of tiny dots with strong contrast enhancement within the dilated intrahepatic bile ducts (the "central dot" sign) is considered very suggestive of Caroli disease (Fig 7) (12). At histopathologic analysis, these intraluminal dots correspond to intraluminal portal vein radicals (12). Intraluminal biliary calculi may be demonstrated.

At MR imaging, the dilated and cystic biliary system appears hypointense on T1-weighted images and markedly hyperintense on T2-weighted images (13). After intravenous administration of gadolinium contrast material, the intraluminal portal vein radicals strongly enhance (13). MR imaging usually demonstrates bridges across dilated intrahepatic ducts, which resemble internal septa (13). This appearance is consistent with the wall of an insufficiently resorbed, malformed ductal plate that surrounds the portal vein radicals. In the absence of the central dot sign, MR cholangiography can be extremely valuable in diagnosis of Caroli disease by demonstrating the pathognomonic feature of saccular dilated and nonob-

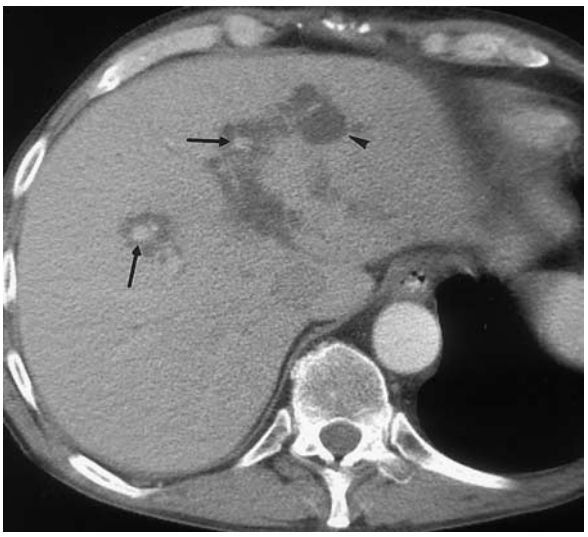

**Figure 7.** Caroli disease in a 54-year-old man. Portal-venous-phase contrast-enhanced CT scan shows saccular dilatation of the biliary tree (arrowhead) with enhancement of central portal vein radicals (arrows) (the central dot sign).

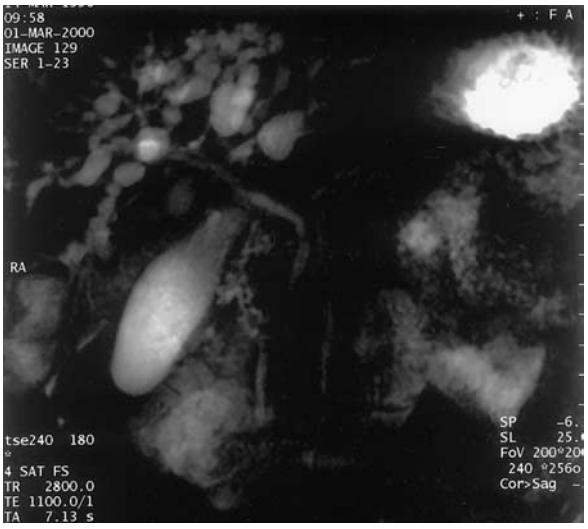


**Figure 8.** Caroli disease in a young girl. Coronal projection MR cholangiogram shows a connection between the saccular dilated segmental bile ducts and the central biliary tree.

structed intrahepatic bile ducts that communicate with the biliary tree (Fig 8) (14).

## Neoplastic Lesions

### Undifferentiated Embryonal Sarcoma

Undifferentiated embryonal sarcoma is a rare malignant hepatic tumor that occurs predominantly in older children and adolescents (mean age, 12 years), although it can occur in young adults as well (15–18).

At cross-sectional imaging, the tumor typically appears as a large (10–25-cm-diameter), solitary, predominantly cystic mass with well-defined borders; occasionally, a pseudocapsule separates the mass from normal liver tissue (15,16). Internal calcifications have been reported sporadically (Fig 9a) (16). Although undifferentiated embryonal sarcoma appears predominantly solid at gross examination (83% of cases) (Fig 9b), CT and MR images usually demonstrate a discordant cystic appearance due to the high water content of the myxoid stroma, which is typical of undifferentiated embryonal sarcoma (18). Therefore, at MR imaging, large portions of the mass are hypointense on T1-weighted images and have high signal intensity on T2-weighted images (Fig 10a) (17,18). Streaky areas of high signal intensity on T1-weighted images and low signal intensity on T2-weighted images represent intratumoral hemorrhage, a feature better appreciated with MR imaging (17,18). On contrast-enhanced CT and MR images, heterogeneous enhancement is present in the solid, usually peripheral portions of the mass, especially on delayed images (Fig 10b) (17,18).

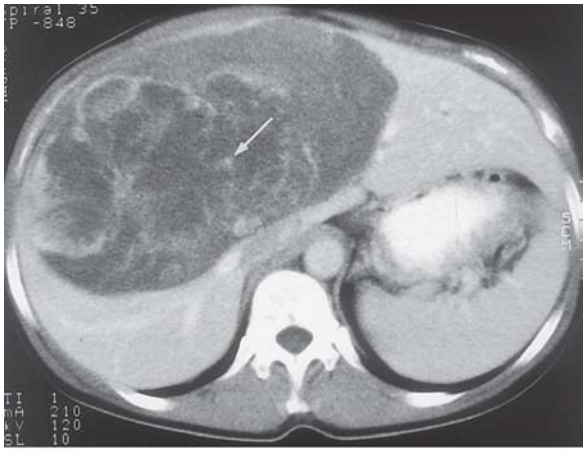

a.

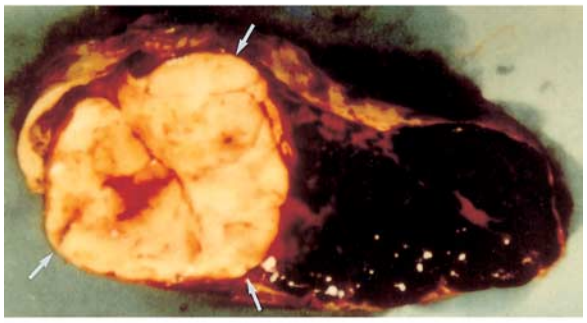

b.

**Figure 9.** Undifferentiated embryonal sarcoma in a 22-year-old woman. **(a)** Portal-venous-phase contrast-enhanced CT scan shows a 10-cm-diameter cystic lesion with septa in the right lobe of the liver. Note the calcifications (arrow) within the mass. **(b)** Photograph shows that the mass has predominantly solid components (arrows) with coexisting hemorrhagic areas.

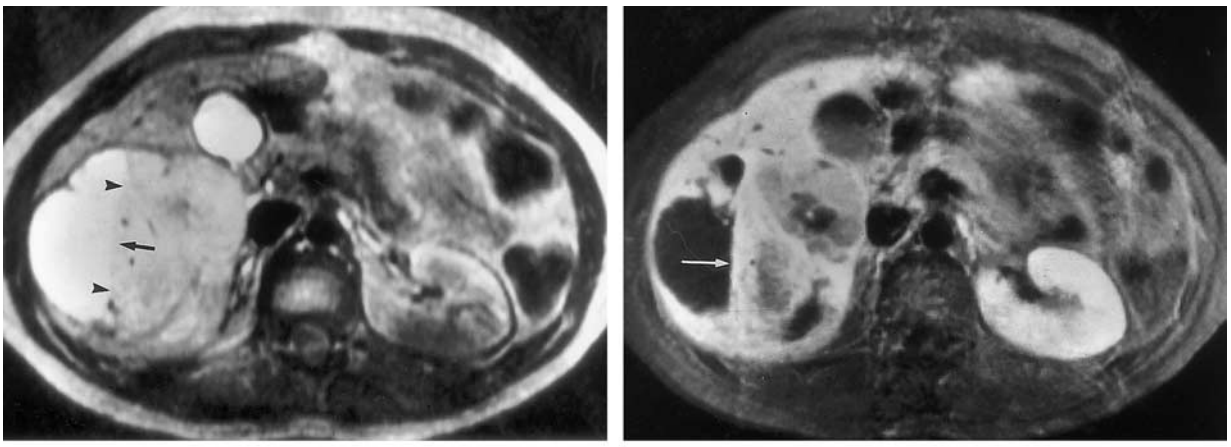

a. b.

**Figure 10.** Undifferentiated embryonal sarcoma in a 36-year-old woman. **(a)** T2-weighted MR image shows a mass in the right lobe of the liver. The solid portions of the mass (arrowheads) are hyperintense relative to normal liver tissue, and the cystic portions (arrow) have signal intensity similar to that of water. **(b)** Delayed-phase gadolinium-enhanced T1-weighted MR image shows heterogeneous enhancement of the solid portions of the lesion (arrow).

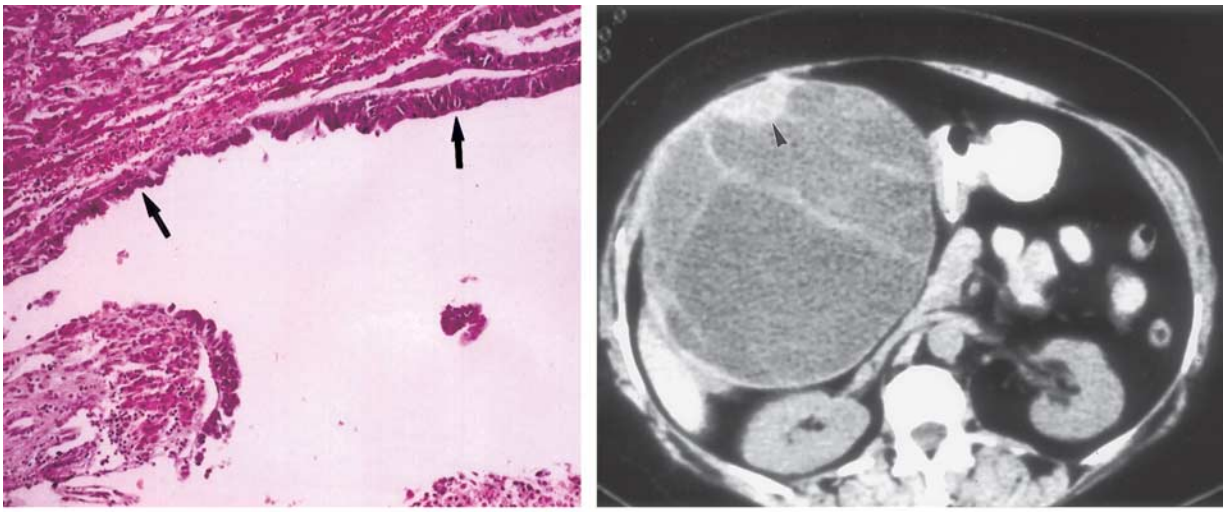

a. b.

**Figure 11.** Biliary cystadenoma. **(a)** Photomicrograph of a biliary cystadenoma shows a monolayer of cuboidal epithelial cells (arrows) delineating the inner space of the cystadenoma. **(b)** Delayed-phase contrast-enhanced CT scan obtained in a 56-year-old woman shows a 12-cm-diameter, multiseptated cystic lesion in the right lobe of the liver. A focal papillary excrescence is noted (arrowhead).

## Biliary Cystadenoma and Cystadenocarcinoma

Biliary cystadenomas are rare, usually slow growing, multilocular cystic tumors that represent less than 5% of intrahepatic cystic masses of biliary origin (1,19,20). Although they are generally intrahepatic (85%), extrahepatic lesions have been reported (19). Among intrahepatic cystadenomas, 55% occur in the right lobe, 29% occur in the left lobe, and 16% occur in both lobes (19). Biliary cystadenomas range in diameter from 1.5 to 35 cm. They occur predominantly in middle-aged women (mean age, 38 years) and are considered premalignant lesions (20). Symptoms are usually related to the mass effect of the lesion and consist of intermittent pain or biliary obstruction (1). At microscopy, a single layer of mucin-secreting cells lines the cyst wall (Fig 11a). The fluid within the tumor can be proteinaceous, mucinous, and occasionally gelatinous, purulent, or hemorrhagic due to trauma (19,20).

At CT, a biliary cystadenoma appears as a solitary cystic mass with a well-defined thick fibrous capsule, mural nodules, internal septa, and rarely capsular calcification (Fig 11b) (19,20). Polypoid, pedunculated excrescences are seen more commonly in biliary cystadenocarcinoma than in cystadenoma, although papillary areas and pol-

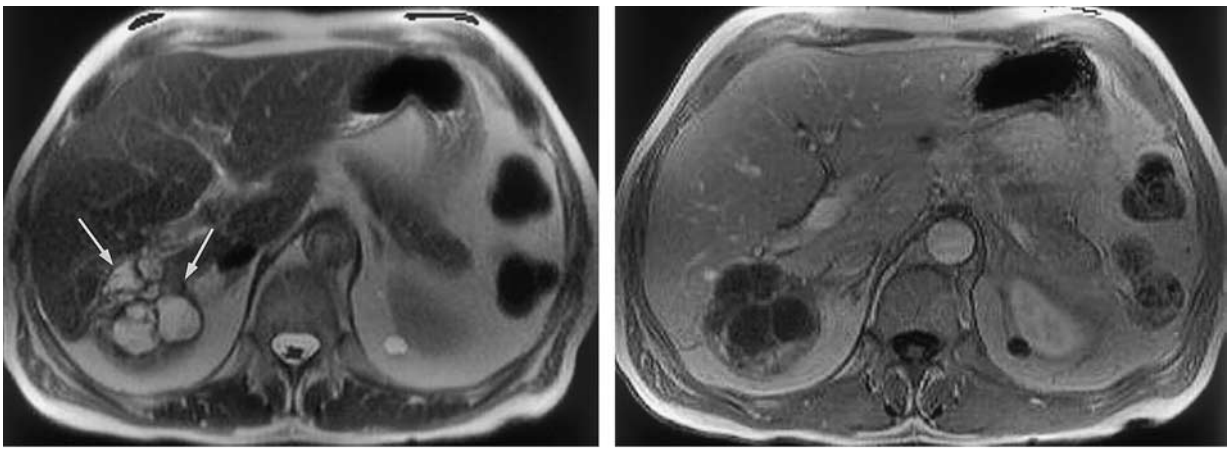

a. b.

**Figure 12.** Biliary cystadenoma in a 49-year-old woman. **(a)** Fast spin-echo T2-weighted MR image shows a multilocular, septated mass (arrows) in segment 7 of the liver, with high signal intensity within the cystadenoma. **(b)** Corresponding portal-venous-phase gadolinium-enhanced T1-weighted MR image shows enhancement of the capsule and septa.

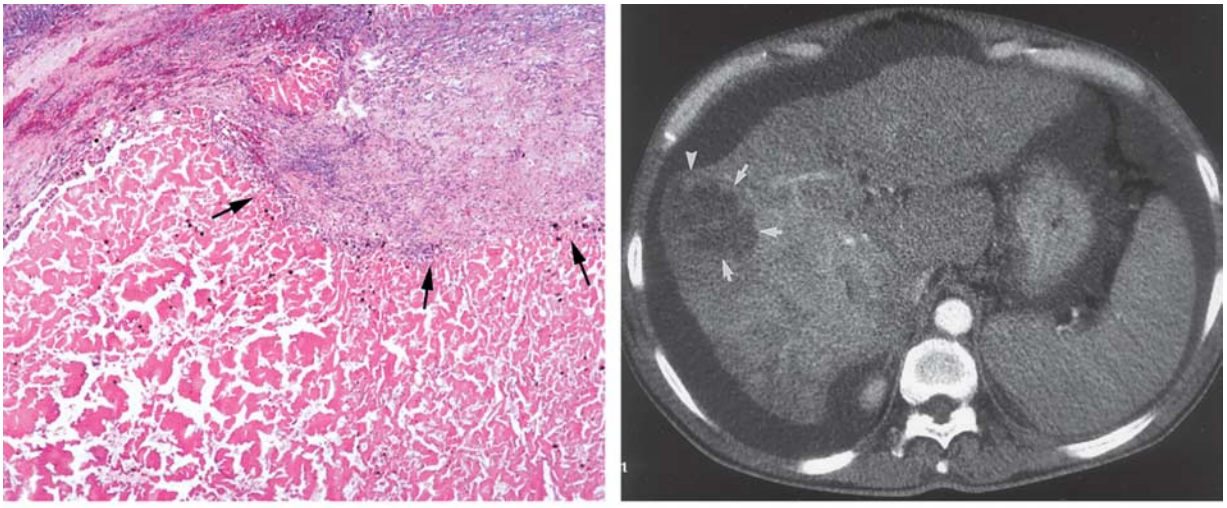

a. b.

**Figure 13.** Cystic hepatocellular carcinoma. **(a)** Photomicrograph of a hepatocellular carcinoma nodule obtained after chemoembolization shows subtotal coagulation necrosis of the lesion with residual viable tumor at the periphery (arrows). **(b)** Arterial-phase contrast-enhanced CT scan obtained in a 55-year-old man shows indirect signs of liver cirrhosis: atrophy of the right hepatic lobe, hypertrophy of the caudate lobe, contour irregularities, and ascites. In addition, an ill-defined cystic mass is seen in the right hepatic lobe (arrows). A small hypervascular nodule is seen at the periphery of the mass (arrowhead).

ypoid projections have been reported in cystadenomas without frank malignancy (15). The MR imaging characteristics of an uncomplicated biliary cystadenoma correlate well with the pathologic features: The appearance of the content is typical for a fluid-containing multilocular mass, with homogeneous low signal intensity on T1-weighted images and homogeneous high signal intensity on T2-weighted images (Fig 12) (19,20). Variable signal intensities on both T1- and T2-weighted images depend on the presence of solid components, hemorrhage, and protein content (19,20).

## Cystic Subtypes of Primary Liver Neoplasms

Cystic subtypes of primary liver neoplasms are rare and are usually related to internal necrosis following disproportionate growth or systemic and locoregional treatment. Hepatocellular carcinoma and giant cavernous hemangioma are the two most common primary neoplasms of the liver that rarely manifest as an entirely or partially cystic mass (Fig 13a).

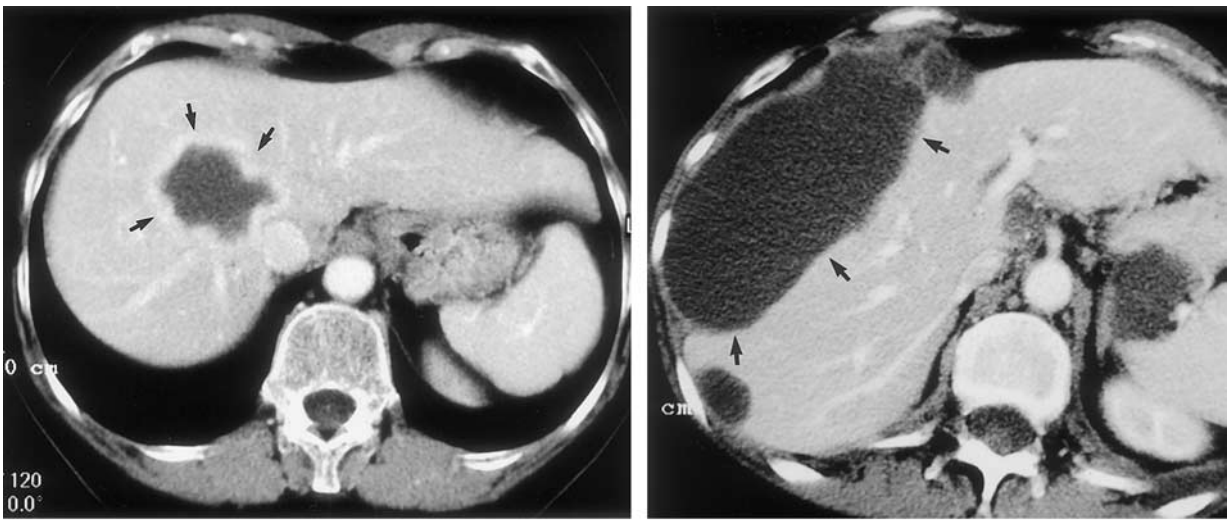


a. b.

**Figure 14.** Cystic metastases. **(a)** Portal-venous-phase contrast-enhanced CT scan obtained in a 42-year-old woman with metastatic breast carcinoma shows a cystic lesion with peripheral enhancement (arrows). **(b)** Portal-venous-phase contrast-enhanced CT scan obtained in a 57-year-old woman shows a 7-cm-diameter elliptical cystic lesion (arrows) on the surface of the liver. This lesion proved to be metastatic ovarian cancer.

In about 70% of patients with hepatocellular carcinoma, CT or MR imaging demonstrates signs or complications of underlying liver cirrhosis, such as hypertrophy of the left hepatic lobe and caudate lobe, regeneration nodules, splenomegaly, and recanalization of the umbilical vein (15). In addition, well-defined intrinsic tumor characteristics of hepatocellular carcinoma may be present, such as hypervascularity of the solid parts, a capsule, and vascular or biliary invasion. The presence of these indirect signs, even in cases in which the predominant component of the tumor is cystic, should suggest the diagnosis (Fig 13b) (1).

Giant cavernous hemangioma can outgrow its blood supply, resulting in central cystic degeneration (21). At CT and MR imaging, a central nonenhancing area is demonstrated within the lesion (21). Since hemangioma has a characteristic peripheral nodular enhancement pattern at both contrast-enhanced CT and contrast-enhanced MR imaging, even lesions with extensive central necrosis are easily diagnosed correctly with both imaging modalities (22).

### Cystic Metastases

Metastases to the liver are common, and a variety of often nonspecific appearances have been reported (23). Most hepatic metastases are solid, but some have a complete or partially cystic appearance (23). In general, two different pathologic mechanisms can explain the cystlike appearance of hepatic metastases. First, hypervascular metastatic tumors with rapid growth may lead to necrosis and cystic degeneration. This mechanism is frequently demonstrated in metastases from neuroendocrine tumors, sarcoma, melanoma, and certain subtypes of lung and breast carcinoma (23). Contrast-enhanced CT and MR imaging typically demonstrate multiple lesions with strong enhancement of the peripheral viable and irregularly defined tissue (Fig 14a) (23). Second, cystic metastases may also be seen with mucinous adenocarcinomas, such as colorectal or ovarian carcinoma (24). Ovarian metastases commonly spread by means of peritoneal seeding rather than hematogenously (25). Therefore, they appear on cross-sectional images as cystic serosal implants on both the visceral peritoneal surface of the liver and the parietal peritoneum of the diaphragm (Fig 14b) (25). This appearance is in contradistinction to that of most other cystic hepatic lesions, which are intraparenchymal.

## Inflammatory Lesions

### Abscess

Abscesses can be classified as pyogenic, amebic, or fungal (26). Pyogenic hepatic abscesses are most commonly caused by *Clostridium* species and gram-negative bacteria, such as *Escherichia coli* and *Bacteroides* species, which enter the liver via the portal venous system or biliary tree (26). Ascending cholangitis and portal phlebitis are the

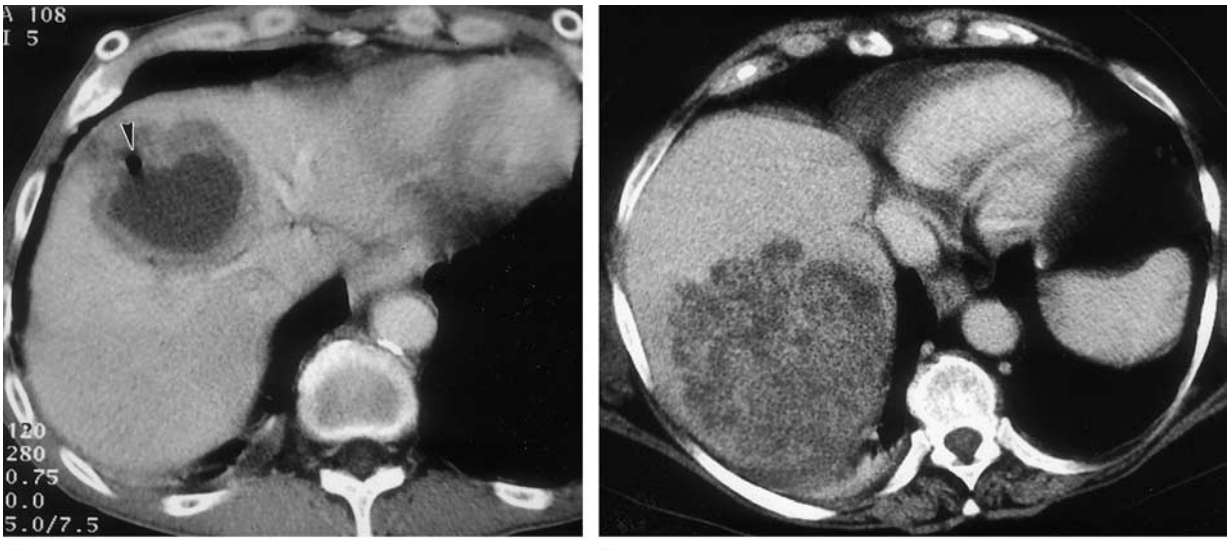


a. b.

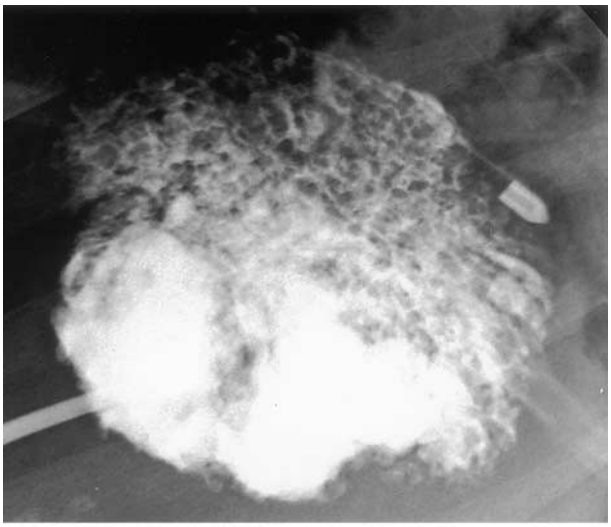

c.

**Figure 15.** Pyogenic abscesses. **(a)** Delayed-phase contrast-enhanced CT scan obtained in a 64-year-old man with fever shows a thick-walled cystic lesion with peripheral enhancement. Note the small pocket of air in the nondependent portion of the mass (arrowhead), which is virtually diagnostic of an abscess due to a gas-forming organism. **(b)** Portal-venous-phase contrast-enhanced CT scan obtained in a 62-year-old woman shows a large cystic mass in segment 8 of the liver. The lesion consists of a confluent cluster of numerous tiny hepatic abscesses. **(c)** Abscessogram (same patient as in **b**) shows opacification of the communicating abscesses.

most frequent causes of pyogenic hepatic abscesses (1). An amebic abscess results from infection with the protozoan *Entamoeba histolytica* and is the most commonly encountered hepatic abscess on a worldwide basis (26). Fungal abscesses are most often caused by *Candida albicans* (26). Clinical symptoms of abscesses are related to the coexistence of sepsis and the presence of one or more space-occupying lesions (1).

In general, the presence of air within a lesion, although uncommon, is diagnostic of a gas-forming organism if there is no history of instrumentation or rupture into a hollow viscus (Fig 15a). Air is easily recognizable at CT by measuring the Hounsfield units (range, −1,000 to −100 HU). At MR imaging, air appears as a signal void and is therefore more difficult to differentiate from calcifications. However, the shape and location (air-fluid level) should enable correct diagnosis. The overall appearance of a hepatic abscess at cross-sectional imaging varies according to the pathologic stage of the infection (26). Abscesses have a unilocular cystic appearance in subacute stages, in which necrosis and liquefaction predominate (26). In more acute stages, abscesses frequently manifest as a cluster of small low-attenuation or high-signal-intensity lesions, which represent different locations of contamination (Fig 15b, 15c) (1). This coalescent, grouped appearance is especially suggestive of pyogenic infection (1).

Abscesses usually appear as thick-walled lesions with homogeneous low attenuation at CT, homogeneous low signal intensity on T1-weighted MR images, and homogeneous high signal intensity on T2-weighted MR images (26,27). In addition to the enhancing abscess wall, contrast-enhanced CT and especially contrast-enhanced MR imaging typically show increased peripheral rim enhancement, which is secondary to increased capillary permeability in

the surrounding liver parenchyma (the "double target" sign) (Fig 16) (1,27). Perilesion edema is seen on T2-weighted MR images in 50% of abscesses, although it may also be seen in 20%–30% of patients with primary or secondary hepatic malignancies (27). Therefore, the presence of perilesion edema can be used to differentiate a hepatic abscess from a benign cystic hepatic lesion (27).

### Intrahepatic Hydatid Cyst

Hepatic echinococcosis is an endemic disease in the Mediterranean basin and other sheep-raising countries (26). Humans become infected by ingestion of eggs of the tapeworm *Echinococcus granulosus*, either by eating contaminated food or from contact with dogs (26). The ingested embryos invade the intestinal mucosal wall and proceed to the liver by entering the portal venous system (26). Although the liver filters most of these embryos, those that are not destroyed then become hepatic hydatid cysts (26). At biochemical analysis, there is usually eosinophilia, and a serologic test is positive in 25% of patients (1). At histopathologic analysis, a hydatid cyst is composed of three layers: the outer pericyst, which corresponds to compressed liver tissue; the endocyst, an inner germinal layer; and the ectocyst, a translucent thin interleaved membrane (Fig 17a) (26). Maturation of a cyst is characterized by the development of daughter cysts in the periphery as a result of endocyst invagination (26). Peripheral calcifications are not uncommon in viable or nonviable cysts (26).

At CT, a hydatid cyst usually appears as a well-defined hypoattenuating lesion with a distinguishable wall (28). Coarse calcifications of the wall are present in 50% of cases (Fig 17b), and daughter cysts are identified in approximately 75% of patients (1,28). MR imaging clearly demonstrates the pericyst, the matrix, and daughter cysts (29). The pericyst is seen as a hypointense rim on both T1- and T2-weighted images because of its fibrous composition and the presence of calcifications (Fig 17c) (26,29). The hydatid matrix (hydatid "sand") appears hypointense on T1-weighted images and markedly hyperintense on T2-weighted images; when present, daughter cysts are more hypointense than the matrix on T2-weighted images (29).

## Miscellaneous Lesions

### Hepatic Extrapancreatic Pseudocyst

Although pancreatic pseudocysts can form anywhere in the abdomen, intrahepatic occurrence is rare (1,30). They occur predominantly in the left lobe of the liver as a result of extension of fluid from the lesser sac into the leaves of the hepatogastric ligament (30). Clinical symptoms are usually related to the underlying inflammatory pancreatic disease. Elevated serum and urinary amylase levels should arouse suspicion for this condition (30).

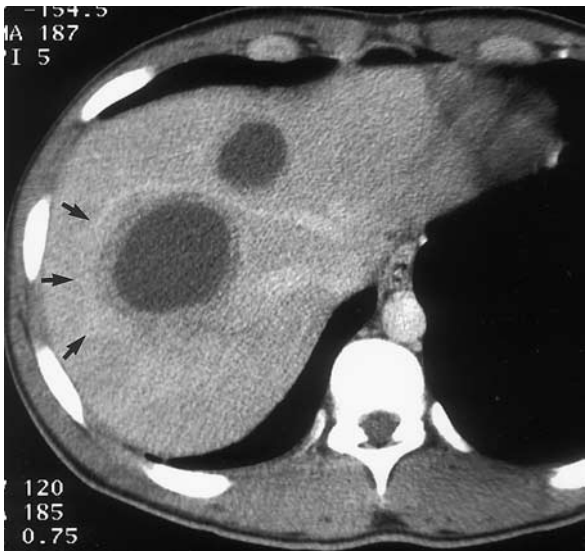


**Figure 16.** Amebic abscess in a 25-year-old man with biopsy-proved hepatic amebiasis. Arterial-phase contrast-enhanced CT scan shows a cystic lesion with high attenuation of the surrounding normal liver parenchyma (arrows) due to hyperemia (the double target sign).

Correct diagnosis is not difficult with imaging when other signs of acute pancreatitis are present (30). At CT, a mature intrahepatic pseudocyst appears as a well-defined, subcapsular, homogeneous, hypoattenuating mass surrounded by a thin fibrous capsule (Fig 18a) (1). In more acute settings, the attenuation of the fluid within the cyst may be higher due to hemorrhage and necrotic debris, and the lesion may be less distinctly defined (1). At MR imaging, a pancreatic pseudocyst appears as a well-circumscribed subcapsular lesion with low signal intensity on T1-weighted images and marked high signal intensity on T2-weighted images (Fig 18b) (31). In mature cysts, an enhancing capsule is seen following intravenous administration of gadolinium chelates (31). Studies that evaluated the usefulness of MR imaging versus CT in patients with pancreatic fluid collections prior to drainage showed that MR imaging is superior for prediction of drainability (31). T2-weighted MR imaging allows better visualization of fluid and solid components within complex collections and therefore provides essential information about the presence or absence of debris that cannot be removed with standard pseudocyst drainage techniques (31).

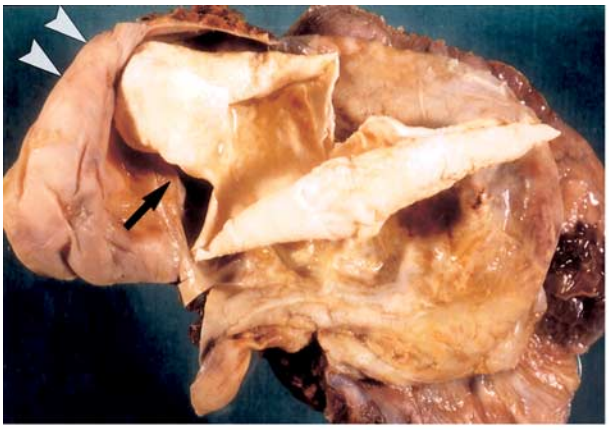

a.

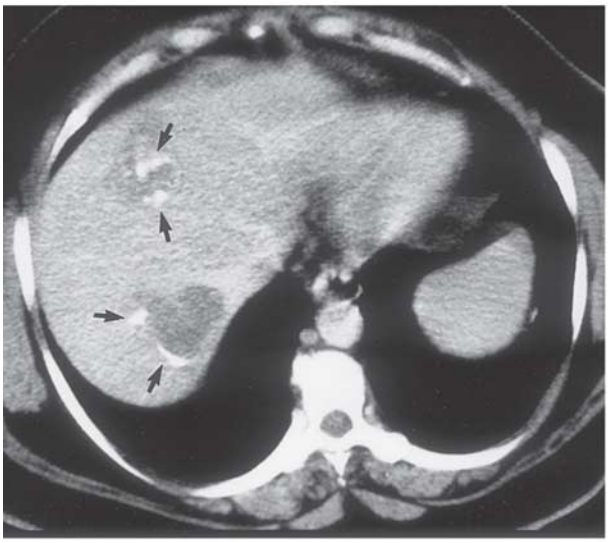

b.

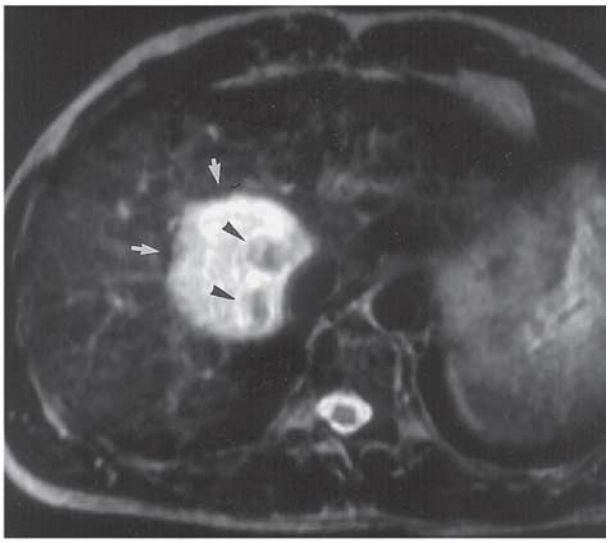

c.

**Figure 17.** Hydatid cyst. **(a)** Photograph of a resected hepatic hydatid cyst shows the fibrous pericyst (arrowheads) and the opened endocyst (arrow). **(b)** Portal-venous-phase contrast-enhanced CT scan obtained in a 45-year-old sheep raiser shows two cystic lesions in the liver with subtotally calcified walls (arrows). **(c)** Fast spin-echo T2-weighted MR image obtained in a 32-year-old man shows a solitary hyperintense lesion in the right lobe of the liver. Note the internal calcifications (arrowheads) and the hypointense pseudocapsule (arrows).

a.

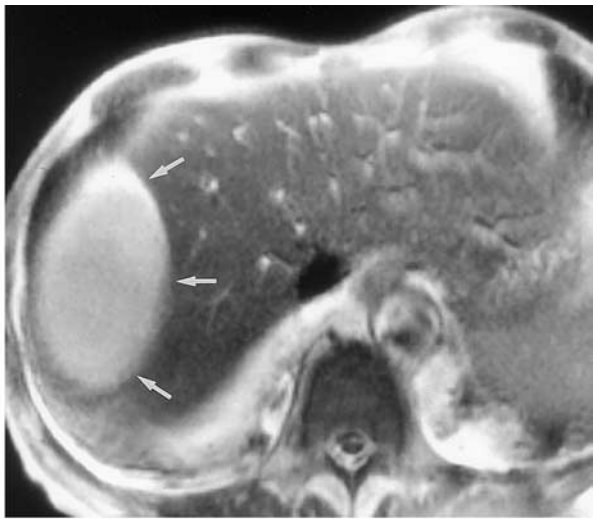

b.

**Figure 18.** Intrahepatic pancreatic pseudocyst. **(a)** Portal-venous-phase contrast-enhanced CT scan, obtained in a 34-year-old patient after an episode of acute severe pancreatitis 3 weeks earlier, shows multiple intraperitoneal pseudocysts and a 5-cm-diameter cystic lesion in the left lobe of the liver (arrows). The lesion is well-defined due to the presence of a capsule, is homogeneous, and in the clinical context is pathognomonic for an intrahepatic pancreatic pseudocyst. **(b)** Half-Fourier acquisition single-shot fast spin-echo T2-weighted MR image obtained in another patient after an episode of necrotizing pancreatitis shows a homogeneous hyperintense pseudocyst (arrows) along the right lobe of the liver.

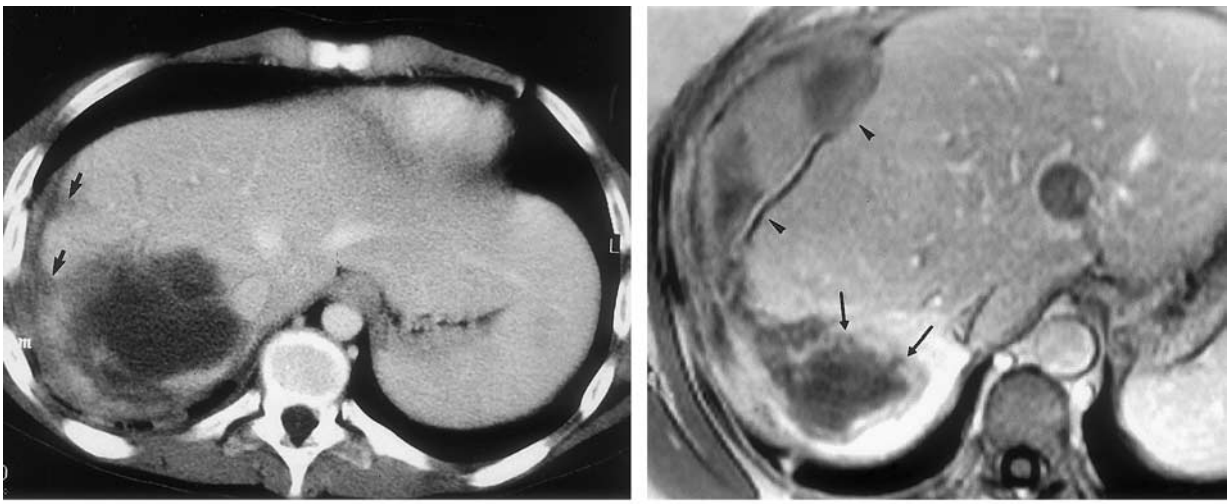

a. b.

**Figure 19.** Hepatic hematoma. **(a)** Portal-venous-phase contrast-enhanced CT scan obtained in a 43-year-old assault victim shows a low-attenuation parenchymal hematoma in the posterior segment of the right hepatic lobe, with coexisting small irregular liver lacerations (arrows). **(b)** Portal-venous-phase gadolinium-enhanced T1-weighted MR image obtained in a 27-year-old woman shows a "cystic" mass (arrows) in the right hepatic lobe with coexistent acute subcapsular hemorrhage (arrowheads). Consequent laparotomy revealed a bleeding hepatocellular adenoma.

## Hematoma

Surgery and trauma are the two most common causes of hepatic bleeding. Hemorrhage within a solid liver neoplasm, especially a hepatocellular adenoma, is a third well-known mechanism by which intra- or perihepatic hematoma can be induced (32). Symptomatic manifestations depend on the severity of the bleeding, the location, and the time frame during which the hemorrhage occurred.

At CT, the appearance of an intrahepatic hemorrhage depends on the cause of the bleeding and the lag time between the traumatic event and the imaging procedure. In an acute or subacute setting, hemorrhage has a higher attenuation value than pure fluid due to the presence of aggregated fibrin components (33). In chronic cases, a hematoma has attenuation identical to that of pure fluid (Fig 19a). Frequently, the cause of the hemorrhage can be detected at CT. In posttraumatic cases, coexistent features such as hepatic lacerations, rib fractures, or perihepatic fluid will be present. In hemorrhage induced by surgery, the location of the hematoma (along the surgical plane) will often be a clue to the diagnosis. The presence of a perihepatic hematoma in combination with a hemorrhagic mass is highly suggestive of hepatocellular adenoma (Fig 19b). Because of the paramagnetic effect of methemoglobin, MR imaging is even more suitable than CT for detection and characterization of hemorrhage. A subacute hematoma appears as a heterogeneous mass with pathognomonic high signal intensity on T1-weighted images and intermediate signal intensity on T2-weighted images (Fig 20) (34).

## Biloma

Bilomas result from rupture of the biliary system, which can be spontaneous, traumatic, or iatrogenic following surgery or interventional procedures (1). Bilomas can be intrahepatic or perihepatic. Extravasation of bile into the liver parenchyma generates an intense inflammatory reaction, thereby inducing formation of a well-defined pseudocapsule. Clinical manifestations depend on the location and size of the biloma (1).

At both CT and MR imaging, a biloma usually appears as a well-defined or slightly irregular cystic mass without septa or calcifications (1). Also, the pseudocapsule is usually not readily identifiable (1). This imaging appearance, in combination with the clinical history and location, should enable correct diagnosis (Fig 21).

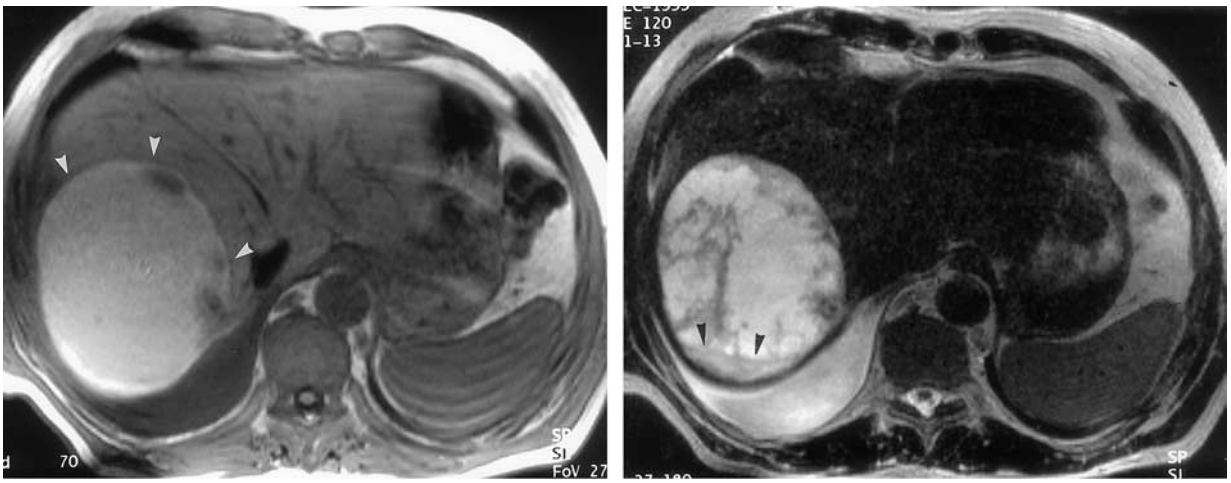

a. b.

**Figure 20.** Hepatic hematoma in a 49-year-old man after a complicated ultrasonographically guided liver biopsy. **(a)** T1-weighted MR image shows a well-defined subcapsular hepatic mass (arrowheads). The high signal intensity within the lesion, which is due to the paramagnetic effect of methemoglobin, is diagnostic for subcapsular hemorrhage. **(b)** Corresponding heavily T2-weighted MR image shows that the mass has high signal intensity and contains internal debris (arrowheads).

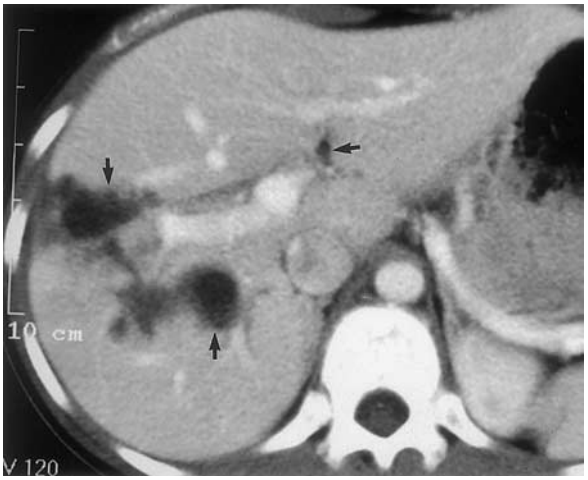

**Figure 21.** Hepatic bilomas in a 21-year-old man with biliary leakage after a severe motor vehicle accident. Follow-up portal-venous-phase contrast-enhanced CT scan shows three intrahepatic collections (arrows) compatible with bilomas. The lesions do not have septa, capsules, or calcifications.

## Conclusions

Characterization of cystic focal liver lesions has always been a challenge for the radiologist. However, due to refined and new imaging techniques, in most cases a correct presumptive diagnosis can be made on the basis of imaging criteria alone. Specific CT and MR imaging findings that are important to recognize are the size of the lesion; the presence and thickness of a wall; the presence of septa, calcifications, or internal nodules; the enhancement pattern; the MR cholangiographic appearance; and the signal intensity spectrum. In addition, access to critical clinical information remains extremely important. The most important clinical parameters defined include age and gender, clinical history, and symptoms.

## References


1. Murphy BJ, Casillas J, Ros PR, et al. The CT appearance of cystic masses of the liver. RadioGraphics 1989; 9:307–322.
2. Singh Y, Winick AB, Tabbara SO. Multiloculated cystic liver lesions: radiologic-pathologic differential diagnosis. RadioGraphics 1997; 17:219–224.
3. Mergo PJ, Ros PR. Benign lesions of the liver. Radiol Clin North Am 1998; 36:319–331.
4. vanSonnenberg E, Wroblicka JT, D'Agostino HB, et al. Symptomatic hepatic cysts: percutaneous drainage and sclerosis. Radiology 1994; 190:387–392.
5. Mathieu D, Vilgrain V, Mahfouz A, et al. Benign liver tumors. Magn Reson Imaging Clin N Am 1997; 5:255–288.
6. Wei SC, Huang GT, Chen CH, et al. Bile duct hamartomas: a report of two cases. J Clin Gastroenterol 1997; 25:608–611.
7. Martinoli C, Cittadini G Jr, Rollandi GA, Conzi R. Case report: imaging of bile duct hamartomas. Clin Radiol 1992; 45:203–205.
8. Wohlgemuth WA, Böttger J, Bohndorf K. MRI, CT, US and ERCP in the evaluation of bile duct hamartomas (von Meyenburg complex): a case report. Eur Radiol 1998; 8:1623–1626.
9. Slone HW, Bennett WF, Bova JG. MR findings of multiple biliary hamartomas. AJR Am J Roentgenol 1993; 161:581–583.
10. Maher MM, Dervan P, Keogh B, Murray JG. Bile duct hamartomas (von Meyenburg complexes): value of MR imaging in diagnosis. Abdom Imaging 1999; 24:171–173.

11. Semelka RC, Hussain SM, Marcos HB, Woosley JT. Biliary hamartomas: solitary and multiple lesions shown on current MR techniques including gadolinium enhancement. J Magn Reson Imaging 1999; 10:196–201.
12. Choi BI, Yeon KM, Kim SH, Han MC. Caroli disease: central dot sign in CT. Radiology 1990; 174:161–163.
13. Zangger P, Grossholz M, Mentha G, Lemoine R, Graf JD, Terrier F. MRI findings in Caroli's disease and intrahepatic pigmented calculi. Abdom Imaging 1995; 20:361–364.
14. Pavone P, Laghi A, Catalano C, Materia A, Basso N, Passariello R. Caroli's disease: evaluation with MR cholangiopancreatography (MRCP). Abdom Imaging 1996; 21:117–119.
15. Powers C, Ros PR, Stoupis C, et al. Primary liver neoplasms: MR imaging with pathologic correlation. RadioGraphics 1994; 14:459–482.
16. Buetow PC, Rao P, Marshall WH. Imaging of pediatric liver tumors. Magn Reson Imaging Clin N Am 1997; 5:397–413.
17. Yoon W, Kim JK, Kang HK. Hepatic undifferentiated embryonal sarcoma: MR findings. J Comput Assist Tomogr 1997; 21:100–102.
18. Buetow PC, Buck JL, Pantongrag-Brown L, et al. Undifferentiated (embryonal) sarcoma of the liver: pathologic basis of imaging findings in 28 cases. Radiology 1997; 203:779–783.
19. Palacios E, Shannon M, Solomon C, et al. Biliary cystadenoma: ultrasound, CT, and MRI. Gastrointest Radiol 1990; 15:313–316.
20. Buetow PC, Midkiff RB. Primary malignant neoplasms in the adult. Magn Reson Imaging Clin N Am 1997; 5:289–318.
21. Vilgrain V, Boulos L, Vullierme MP, Denys A, Terris B, Menu Y. Imaging of atypical hemangiomas of the liver with pathologic correlation. RadioGraphics 2000; 20:379–397.
22. Semelka RC, Sofka CM. Hepatic hemangiomas. Magn Reson Imaging Clin N Am 1997; 5:241–253.
23. Lewis KH, Chezmar JL. Hepatic metastases. Magn Reson Imaging Clin N Am 1997; 5:319–330.
24. Sugawara Y, Yamamoto J, Yamasaki S, Shimada K, Kosuge T, Sakamoto M. Cystic liver metastases from colorectal cancer. J Surg Oncol 2000; 74:148–152.
25. Lundstedt C, Holmin T, Thorvinger B. Peritoneal ovarian metastases simulating liver parenchymal masses. Gastrointest Radiol 1992; 17:250–252.
26. Mergo PJ, Ros PR. MR imaging of inflammatory disease of the liver. Magn Reson Imaging Clin N Am 1997; 5:367–376.
27. Mendez RJ, Schiebler ML, Outwater EK, et al. Hepatic abscesses: MR imaging findings. Radiology 1994; 190:431–436.
28. De Liego J, Lecumberri FJ, Francquet T, et al. Computed tomography in hepatic echinococcosis. AJR Am J Roentgenol 1982; 13:699–702.
29. Marani SA, Canossi GC, Nicoli FA, et al. Hydatid disease: MR imaging study. Radiology 1990; 175: 701–706.
30. Okunda K, Sugita S, Tsukada E, et al. Pancreatic pseudocyst in the left hepatic lobe: a report of two cases. Hepatology 1991; 13:359–363.
31. Morgan DE, Baron TH, Smith JK, Robbin ML, Kenney PJ. Pancreatic fluid collections prior to intervention: evaluation with MR imaging compared with CT and US. Radiology 1997; 203: 773–778.
32. Casillas VJ, Amendola MA, Gascue A, Pinnar N, Levi JU, Perez JM. Imaging of nontraumatic hemorrhagic hepatic lesions. RadioGraphics 2000; 20: 367–378.
33. Merrine D, Fishman EK, Zerhouni EA. Spontaneous hepatic hemorrhage: clinical and CT findings. J Comput Assist Tomogr 1988; 12:397–400.
34. Balci NC, Semelka RC, Noone TC, Ascher SM. Acute and subacute liver-related hemorrhage: MRI findings. Magn Reson Imaging 1999; 17: 207–211.

*This article meets the criteria for 1.0 credit hour in category 1 of the AMA Physician's Recognition Award. To obtain credit, see www.rsna.org/education/rg_cme.html.*